IPP-Report

IPP Max-Planck-Institut für Plasmaphysik

Hans Kastelewicz, Ralf Schneider,
David Coster and Detlev Reiter

A Numerical Model for the PSI-1 Linear Plasma Device

Ein numerisches Modell für den linearen Plasmagenerator PSI-1

IPP 8/16
März 2000

MAX - PLANCK - INSTITUT FÜR PLASMAPHYSIK

GARCHING BEI MÜNCHEN

A Numerical Model for the PSI-1 Linear Plasma Device

H. Kastelewicz, R. Schneider[1*],
D. Coster[1], and D. Reiter[2]

IPP 8/16 March 2000

Humboldt-Universität zu Berlin, Institut für Physik, 10115 Berlin

[1]Max-Planck-Institut für Plasmaphysik, EURATOM Association
85748 Garching

[1*]Max-Planck-Institut für Plasmaphysik, EURATOM Association
Teilinstitut Greifswald, 17489 Greifswald

[2]Forschungszentrum Jülich GmbH, Institut für Plasmaphysik
52425 Jülich

A Numerical Model for the PSI-1 Linear Plasma Device

H. Kastelewicz, R. Schneider, D. Coster, D. Reiter

Abstract

In the PSI-1 linear device the plasma is generated by a ringshaped arc discharge that builts up pronounced hollow density and temperature profiles. Outside the source along the magnetic field axis, these profiles are strongly modified due to radial diffusion, axial streaming and the interaction with the neutral background.

The presented model is based on the B2–Eirene code package and provides a largely selfconsistent description of the plasma in PSI-1 in dependence on external parameters which are closely related to the experimental ones: The gas influx rate, the pumping efficiencies and the electron source temperature (replacing the experimental discharge power). The detailed plasma generation in PSI-1 by the arc discharge is simulated in the model by explicitely describing the electron energy source due to the discharge current through the measured or fitted source temperature.

The model is applied to a deuterium plasma and quantitatively tested by comparing the calculated electron/ion and neutral densities and temperatures with experimentally measured profiles. The influence of the axial inhomogeneity of the magnetic field on the plasma dynamics and the radial diffusion described by different diffusion laws are studied in detail.

For the magnetic field configuration of PSI-1, the variation of the field strength is found to modulate clearly the axial profiles of the ion velocity, density and temperature, which can be explained by the hydrodynamic behaviour of the plasma; but also the electron temperature is strikingly affected by the field inhomogeneity via the radial energy losses in connection with the nonlinear dependence of the heat conductivity on T_e.

To approximate the experimental radial plasma profiles, a radial diffusion coefficient of the order of $1m^2/s$ is required which is essentially supplied by the considered classical and empirical diffusion laws. In the predominant radial plasma layers, a good quantitative agreement between the calculated and experimental results is obtained then, but there are still problems to reproduce quantitatively the profiles near the column axis and in the anode shadow by any simple diffusion ansatz. This may be due to the neglect of an internal electric field in the B2 code which can influence the radial transport.

1. Introduction

The linear plasma generator PSI-1 / 1 / like similar devices / 2, 3 / are primarily designed to study problems of plasma-surface interactions at high ion flux densities relevant for controlled fusion research.

In PSI-1 (Fig. 1) a high current arc between a ring-shaped cathode and an hollow anode is used to produce an axisymmetric steady-state plasma column of 1.8 m length and 5 to 10 cm diameter which is radially confined by an axial magnetc field ($0.05 \leq B/T \leq 0.1$).

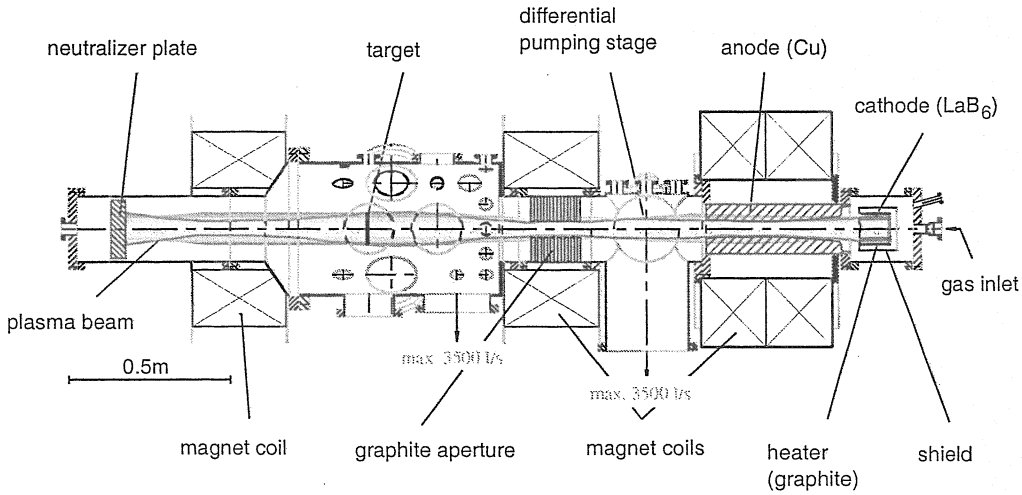

Fig.1 Scheme of the PSI-1 device

The cylindrical vessel ($10 \leq r/cm \leq 20$) consists of stainless steel, the target plate is made of graphite. Graphite diaphragms allow for differential pumping.
The plasma column extending from the anode exit to the neutralizer plate is usually free of external electric fields but, in order to study energy dependent surface processes, targets introduced into the plasma may also be biased.

Several diagnostics (He beam diagnostics, fast Langmuir probe, Thomson scattering, LIF) are used to determine the plasma and neutrals parameters, mainly in the target chamber (see Fig.1). The achievable electron density and temperature depend on the discharge conditions (discharge current / input power and neutral influx rate / pressure) and the working gas and are in the ranges $10^{11} \leq n_e/cm^{-3} \leq 10^{14}$, $T_e \leq 10eV$ / 1 /. The neutral pressure may vary in order's $10^{-2} \leq p/Pa \leq 1$.

Because of the particular ring-shaped design of the anode-cathode system and the effect of the magnetic field the plasma is actually generated off-axis within a narrow shell near the inner anode surface. As a consequence, pronounced hollow radial profiles are built up for the plasma density and temperature which may essentially be modified downstream the plasma column due to radial diffusion, axial streaming and the interaction with the neutrals background (recycling). Experimentally, a rotation of the whole plasma around the symmetry axis is also observed which, however, will be beyond the present model.

The aim of this paper is to give a self-consistent description of the plasma including electrons and ions as well as the neutral gas background in order to better understand the plasma behaviour on the basis of the underlying elementary processes and transport properties. In particular,

several radial transport models will be considered and the influence of the inhomogeneity of the axial magnetic field is studied in detail. Under the supposed plasma conditions, the B2–Eirene code package / 4, 5 / seems a suitable tool for the calculations, treating the plasma ions hydrodynamically and the neutrals on a kinetic basis. On the other hand, in view of the rather comprehensive experimental data set obtained for the plasma species as well as for the neutrals under steady state conditions in PSI-1, the calculations may provide some validation of the code itself, which is also widely used for the much more complicated fusion devices.

2. PSI-1 Model System

In this paper, the B2–Eirene coupled code package is used to describe the combined system of plasma and neutrals in the PSI-1 device for a pure deuterium plasma.

B2 / 6, 7 / is a 2d multifluid plasma code which treats the ion motion parallel to the magnetic field as an hydrodynamic flow and the motion in the radial direction (orthogonal to field lines) as a diffusion process. Accordingly, the calculational grid is defined by the magnetic field produced by the four coils shown in Fig.1. It is calculated using the Sonnet grid generator. The parallel (axial) coordinate lines are given by the magnetic flux surfaces and the radial lines by their orthogonals. Because of the rotational symmetry only half of the axial cross section ranging from the symmetry axis ($r = 0$) up to the wall side need to be considered.

Eirene / 8 / is a 3D Monte-Carlo code for the neutrals. It takes into account the real geometry of the device (the particle trajectories are followed within the whole device), all essential interaction processes between the neutrals and the plasma and the surface processes. Analogous to the experiment, the working gas (D_2) enters the device through a concentric hole in the basic plate of the cathode at room temperature and is pumped in the differential pumping stage and the target chamber. Influx rate and pumping efficiencies are given by the experiment and are external parameters of the model.

Since no electric fields and currents are allowed in the present version of B2 (in this model $n_e = \sum_i n_i$ and $n_e v_e = \sum_i n_i v_i$, where n_e, n_i, v_e, v_i are the densities and velocities of electrons and ions, respectively), the discharge region itself cannot be described consistently. However, since we are primarily interested in the produced plasma and not in the details of the discharge, we may circumvent this problem by explicitely prescribing the electron energy source of the plasma produced by the discharge current / 9 /. The latter is essentially bound to magnetic field lines and thus strongly localized to a narrow shell near the inner anode surface. The spatial distribution of the energy source may thus reasonably be approximated as outlined in Fig. 2 (for example by a step function) while the total energy transfer rate is treated as an external parameter. (The latter is not identical with the total input power given by the discharge current and the externally applied voltage, which also includes. e.g., energy losses to the anode surface by the non-ambipolar current.)

On the understanding not to treat the arc discharge explicitely in this model, some geometrical details in the anode-cathode region can further be simplified since they don't effect the code results significantly (apart from local modifications): The protruding structure of the cathode will be neglected and the inner surface of the anode is assumed to be identical with an axial coordinate line. This simplifies appreciably the boundary conditions for B2 (cf. Fig. 2).

The problem of electric currents has been avoided in an earlier work / 10 / by restricting the calculation to the current-free plasma column outside the anode only. In this case, however,

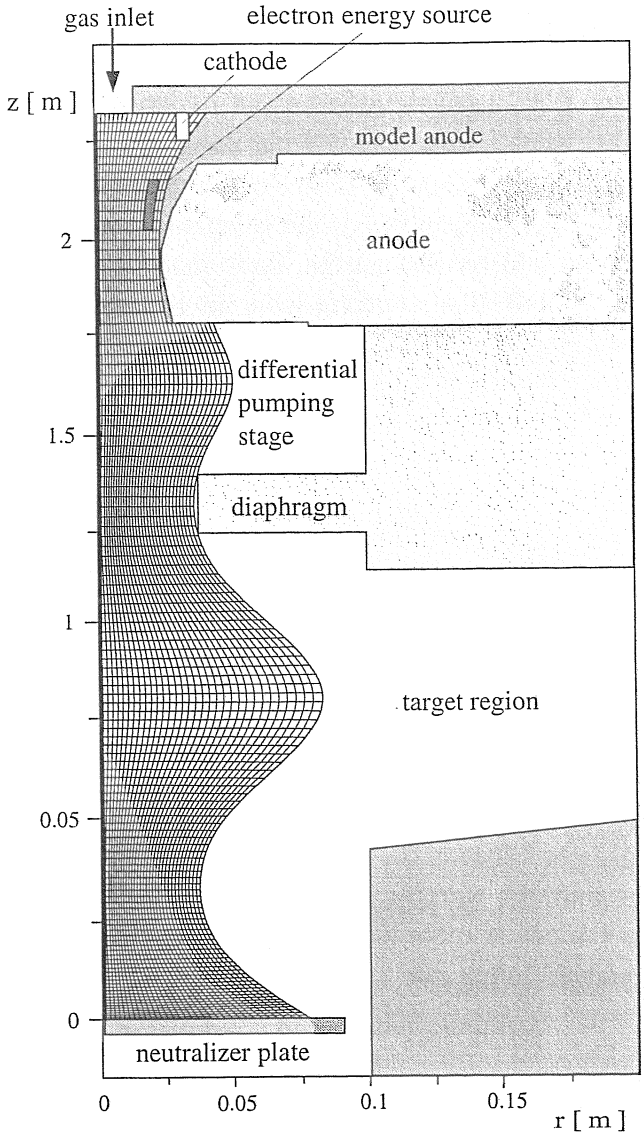

Fig.2 Schema of the PSI-1 model system

boundary conditions had to be postulated at the anode exit for all plasma parameters (i.e., radial functions for the temperatures, densities and ion velocities) which are in general unknown and hardly to estimate. In the present model, the external parameters are the neutral gas influx rate and the pumping efficiencies – which are given experimental quantities – and the electron energy source strength. The latter may likewise be replaced by the electron temperature in the source region.

2.1 B2 Boundary Conditions

Boundary conditions have to be formulated for the electron and ion temperatures (T_e, T_i) and the densities (n_i) and parallel velocities ($u_{p,i}$) for all ion species along the borders of the grid in Fig.2.

At the wall side of the grid a decay length of $1cm$ for all quantities is assumed . Test calculations show that other physically reasonable conditions (for example constant plasma parameters) may

also be chosen without changing the physical results within the plasma volume. The solution adapts to the boundary conditions just in the outer cells of the grid.

At the neutralizer plate and at the cathode bottom "sheath conditions" are used assuming $u_p \geq c_s$ (c_s = sound velocity), energy transmission factors of $\beta_e = 4.0$, $\beta_i = 2.5$ for electrons and ions, respectively, and vanishing density gradient ($\frac{\partial n_i}{\partial x} = 0$). These conditions are formally also applied for the small gas inlet hole; other conditions (for instance free outflow of ions, i.e., $\beta_e = \beta_i = 1$, $u_p = c_s$) yield practically the same results.
Along the symmetry axis of the device the condition of vanishing radial gradients is imposed.

2.2 Radial Transport

In plasma devices with magnetic confinement the cross-field ion diffusion is usually described by anomalous, empirically determined diffusion coefficients (constant values or the Bohm diffusion coefficient, $D_B = T_e[eV]/16B[T]m^2s^{-1}$) which are found to be of the order of $D_i \approx 1m^2/s$. This is much higher than the theoretically derived classical coefficients. Since in PSI-1 the neutral density is rather high (same order of magnitude as the ion density) and the magnetic field is low the classical ion diffusion or the ambipolar diffusion coefficients may also be reasonable assumptions. Therefore, for the deuterium plasma, the following cases are tested here which give coefficients D_i of essentially the same order of magnitude:

$D_i = const = \left[\, 0.5m^2/s\,,\quad 1.0m^2/s\,\right]$,

$D_i = D_{cl-ion} = \frac{r_c^2}{2}\nu_{i,n}$ (classical ion diffusion) where

$\nu_{i,n} = 2.08 \times 10^{-8} cm^3/s \times (n_D + n_{D_2})$ (elastic ion-neutral collision rate / 11 /) and

$r_c = 1.442 \times 10^4 \sqrt{T_i[eV]}\,/B[T]\ m$ (ion cyclotron radius),

$D_i = D_{cl-ambi} = \frac{r_c^2}{2}\nu_{i,n}\left(1 + \frac{T_e}{T_i}\right)$ (classical ambipolar diffusion),

$D_i = 0.03 \times 10^{-4}(T_e/eV) \times \left(\nu_{i,n}/s^{-1}\right) m^2/s$ (empirically found at PISCES / 2 /)

For the radial thermal conductivities and the ion viscosity the following assumptions are made throughout: $\kappa_{e,i}/n_{e,i} = 1m^2/s$ and $\eta_i/m_i n_i = 0.2m^2/s$.

3. Deuterium Plasma

3.1 Dependence on the Model Parameters

The model contains adjustable parameters (temperature and extension of the primary energy source, diffusion coefficient) which can be optimized in order to fit the calculated to the experimentally measured radial plasma profiles at different axial positions. While the source electron temperature controls rather directly the electron temperature in the plasma column the radial source dimension predominantly affects the absolute value of the electron density and D_i determines the shape of the radial profile. (To some extent these effects interfere, of course.)

First we consider code solutions for different diffusion coefficients. These calculations have been done for a total gas influx rate of $F_{D_2} = 2.83 \times 10^{19} molecules/s$ and an assumed source temperature of $T_{e,source} = 12eV$ within a concentric ring of $\Delta_{source} = 4mm$ thickness near the anode surface (Fig.2). The pumping rates are $500l/s$ and $3500l/s$ at the differential pumping stage and at the target chamber, respectively.

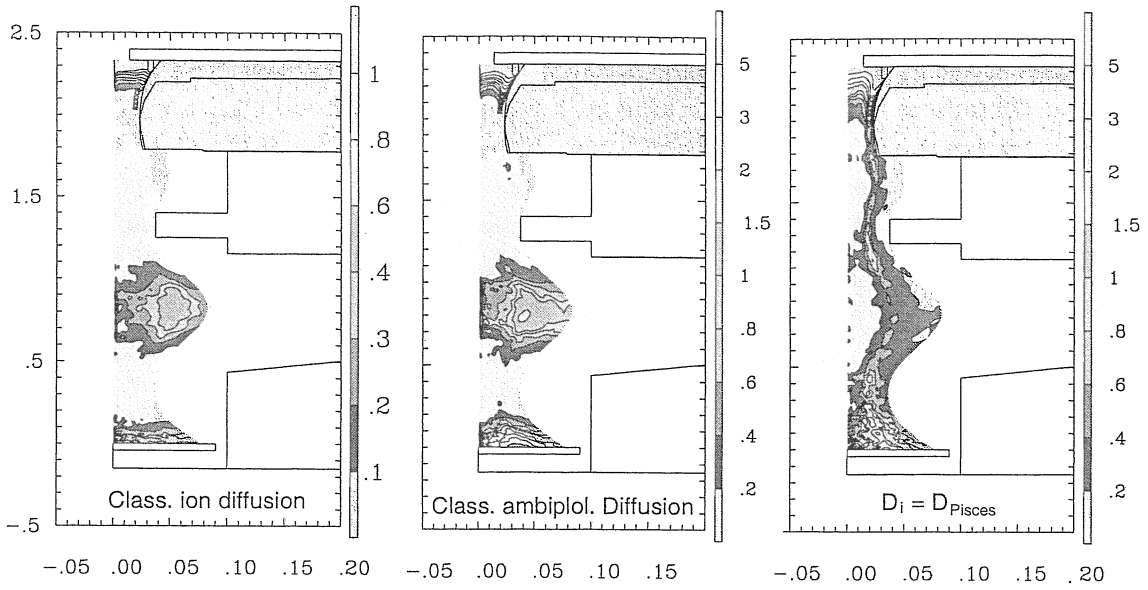

Figs.3 Contour plots of the radial diffusion coefficient
for different diffusion laws (self-consistently calculated)

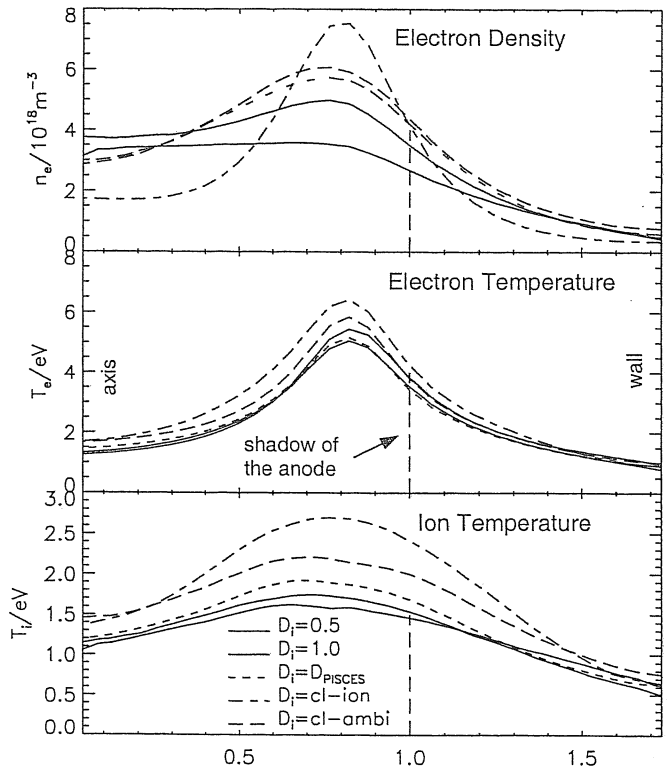

Fig.4 Radial plasma profiles in the target plane
for different diffusion laws and $\Delta_{source} = 4mm$
(in normalized coordinates, see text)

The classical diffusion coefficients and D_{PISCES} depend on the magnetic field strength and the local plasma parameters (and, hence, on the model solution itself) and are self-consistently calculated (Figs. 3).

The classical ion diffusion is least efficient. $D_i\left[m^2/s\right]$ is about 0.5 in the target chamber and at the neutralizer plate (low magnetic field) and $\gtrsim 1$ near the cathode (high neutrals density, large $\nu_{i,n}$); in the other part of the plasma it is less than 0.1. The ambipolar diffusion coefficient behaves similar, but is generally larger (e.g., about 2.5 in the target chamber) since $T_e \geq T_i$. The diffusion coefficient derived at PISCES / 2 / is independent on the magnetic field and is largest in the hot part of the plasma column ($D_i \propto T_e$). $D_i\left[m^2/s\right]$ is about 0.3 in the target chamber and ≈ 2 and $\gtrsim 5$ at the neutralizer plate and at the anode bottom, respectively, where the neutrals density is high.

Some radial plasma profiles in the target plane obtained for the different diffusion assumptions are shown in Fig.4. Here and in the corresponding figures below we use normalized coordinates, where $r = 1$ is defined by the magnetic flux surface touching the inner anode surface (apperture).
The electron density differs at maximum by a factor of 2 for the various D_i models. The most radially peaked hollow profile is obtained for the classical ion diffusion law while for $D_i = const. = 1.0m^2/s$ the radial profile has already become monotoneous at the target plane.

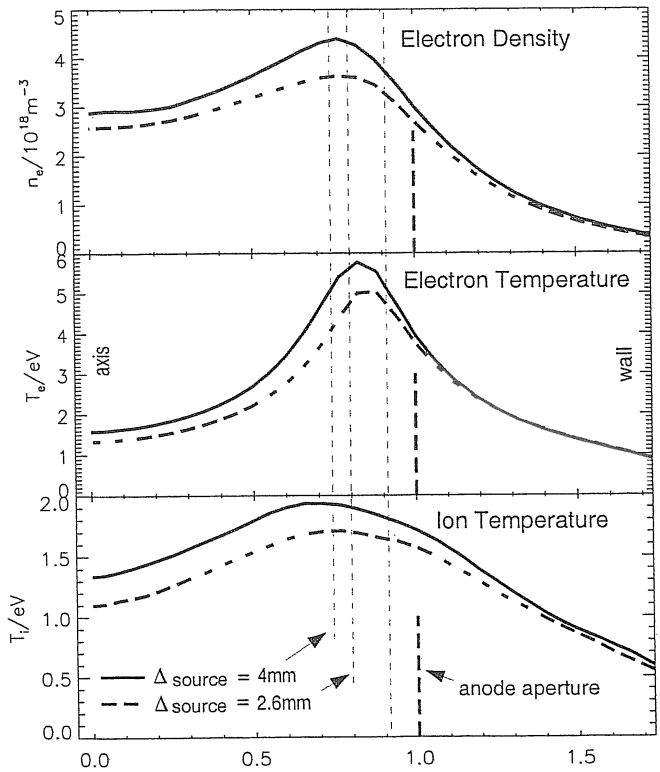

Fig.5 Radial plasma profiles in the target plane for different radial extensions ($\Delta_{source} = 2.6mm$ and $\Delta_{source} = 4mm$) of the primary electron energy source (constant diffusion coefficient $D_i = 0.5m^2/s$)

The influence of the radial source dimension on the calculated plasma profiles is shown in Fig.5, assuming $D_i = 0.5m^2/s$. Apart from a small shift of the temperature profiles, only the absolute height of the profiles is significantly affected as a consequence of the different total input

energy. The axial length of the assumed source is about 10cm and kept fixed in the following. Variations within reasonable limits have no noticeable influence on the solution.

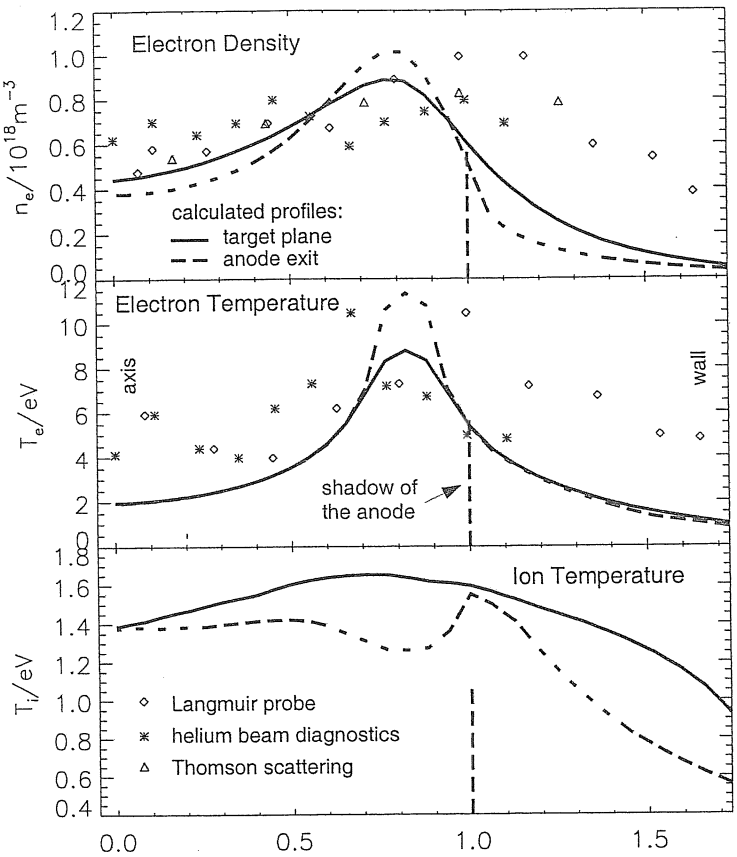

Fig.6 Measured plasma profiles in the target plane obtained with different diagnostics: Langmuir probe ($\diamond$), helium beam diagnostics ($*$), Thomson scattering ($\triangle$). The curves are calculated profiles in the target plane (full line) and at the anode exit (projected along the magnetic flux surfaces to the target plane – broken line).

Fig.6 shows experimentally measured electron density and temperature radial profiles of the plasma column in the target plane and calculated curves obtained for the following parameters: $D_i = 0.5m^2/s$, $F_{D_2} = 1.25 \times 10^{19} molecules/s$, $T_{e,source} = 12eV$, $\Delta_{source} \approx 4mm$ and pumping rates of $1000l/s$ and $3500l/s$ at the differential pumping stage at the target chamber, respectively. There is a fairly good quantitative agreement of the n_e profiles in the main part of the plasma column (within the projection of the anode aperture), so $D_i = 0.5m^2/s$ may be an appropriate choice there, while in the outer part of the column the decrease of the experimental data is too smooth in order to be modelled by the same diffusion coefficient. However, the experimental data also scatter appreciably, so a definite conclusion about the diffusion coefficient will be difficult. Similar arguments apply to the electron temperature.

It should be noted, that changing the radial decay length for the boundary conditions at the wall side of the grid has no effect on this behaviour and influences only the radial plasma profile within the very outer layers of the calculational grid.

For the detailed discussion of the hydrogen plasma in the next chapters the following parameters are used for the calculations which are within the usual PSI-1 working regime:

Gas inlet rate: $F_{D_2} = 2.83 \times 10^{19} molecules/s$
Puming rates: $1000 l/s$ (differential pumping stage) and $3500 l/s$ (target chamber).

The external arc power is replaced by the model parameters:
$T_{e,source} = 12eV$, $\Delta_{source} = 2.6mm$

Moreover, $D_i = 0.5m^2/s$ and the other transport coefficients and boundary conditions summarized above are assumed.

3.2 Charged Particles

In the following chapters a steady state solution of the PSI-1 plasma model for the parameters given above is considered in detail. Some basic plasma parameters are shown in Figs. 7–8. As may be seen from the contourplots (Fig. 7) the hollow T_e profile originating from the radially localized energy source (fixed temperature) near the anode surface is sustained throughout the whole plasma column which is mainly a consequence of the high parallel electron heat conductivity.

The electron density profile is determined by the balancing effects of ioniztion in the high temperature region (mainly inside but also outside the anode, see Fig. 15), radial relaxation due to diffusion and the axial plasma flow. In the considered case it remains hollow up to the dump entrance, since due to the small ion mass in the case of deuterium the parallel ion velocity (Fig. 10) is high and the transit time of the ions too short for an effective relaxation. This is different for the heavier noble gas plasmas.
Else than for T_e and n_e, the contour pattern of the ion temperature is rather complicated due to the mutual exchange of thermal and kinetic energy as will be discussed below.

Fig. 8 shows calculated radial profiles for T_e and n_e in normalized coordinates at different axial positions and, for comparison, experimental curves at the target plane obtained by fast Langmuir probe measurements / 12 / for a $374\,A$ total electric current discharge. The gas influx rate $F_{D_2} = 2.83 \times 10^{19} molecules/s$ and the pumping efficiencies ($1000\,l/s$ and $3500\,l/s$) used in the calculation are the same as in the experiment, while the other (intrinsic) model parameters are asumed to be $T_{e,source} = 11\,eV$, $\Delta_{source} = 2.6\,mm$ and $D_i = 0.5$ for $r/r_s \leq 1$, $D_i = 0.5\,n_e(r_s)/n_e$ for $r/r_s > 1$.
Although there is a good quantitative agreement between the calculated and measured electron density (and temperature, respectively) next to the profile maximum, the density values at the column axis and in the outer plasma region (anode shadow) differ by a factor of almost two. This discrepancy, however, may certainly be removed by better fitting the diffusion coefficient. The more serious differences between the calculated and measured T_e-profiles in the central and outer plasma region, on the other hand, cannot be resolved by changing the radial heat conductivity within reasonable limits. In particular, the electron temperature increase found experimentally in the target plane outside the main plasma column (on magnetic flux surfaces outside the anode apperture) is not understandable. The T_e maximum lies far in the anode shadow which cannot be verified by the model.

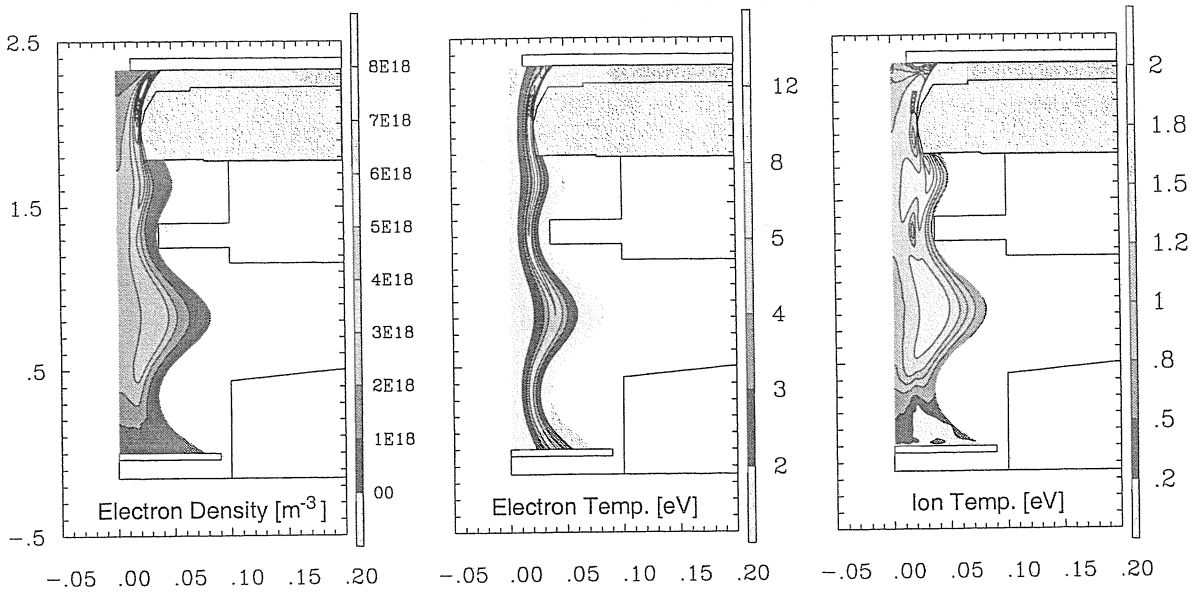

Fig. 7 Contour plots of the electron density and temperature and the ion velocity

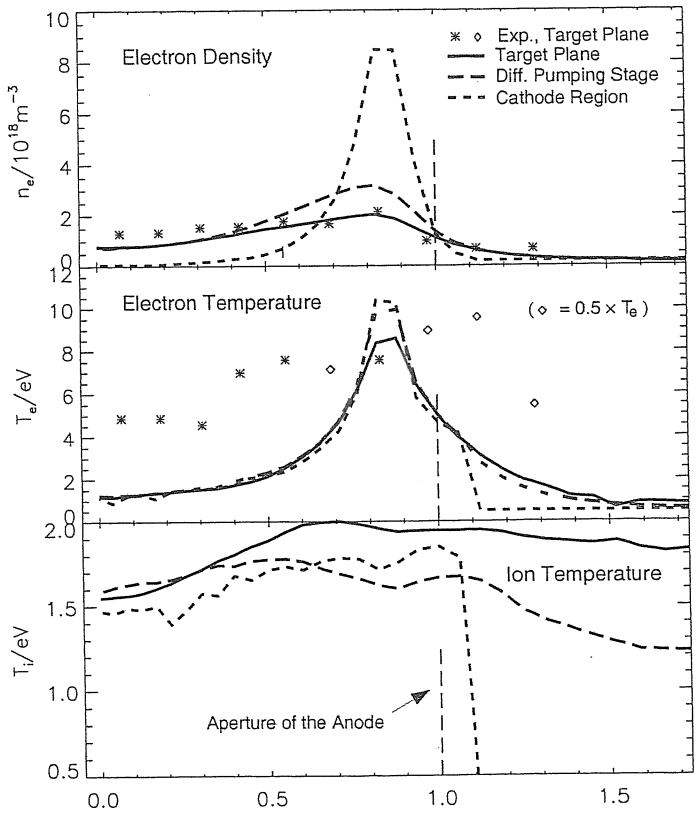

Fig. 8 Radial density and temperature profiles at different axial positions projected along the magnetic field lines onto the target plane. The normalized radial coordinate is defined by the ratio r/r_s, were r_s is the radius of the outmost magnetic flux surface in the target plane which still passes the anode apperture.

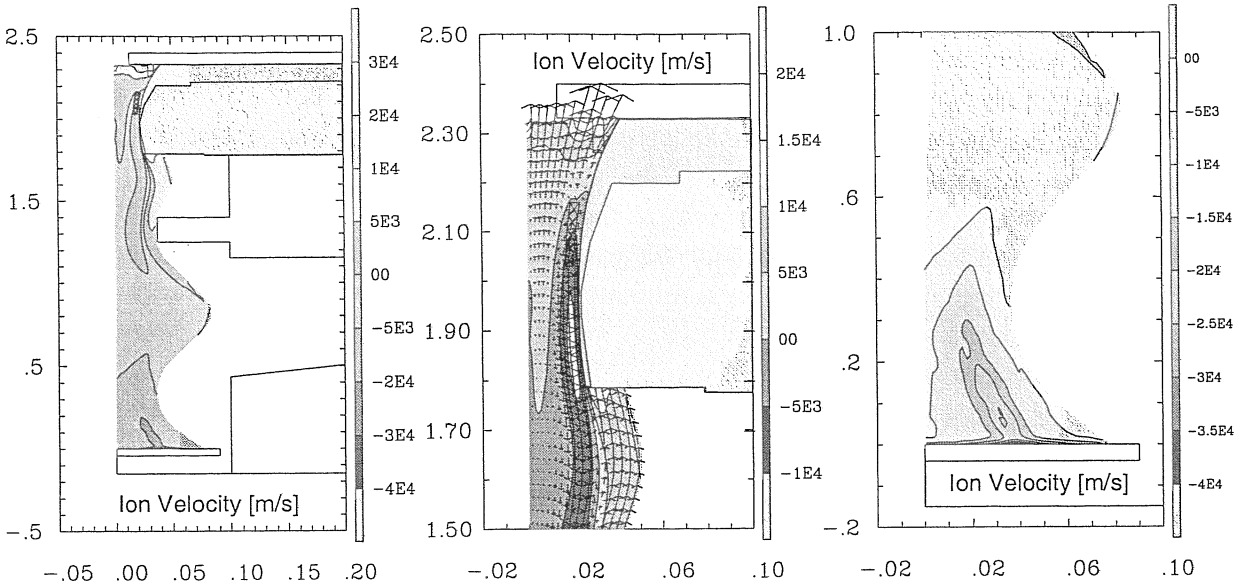

Fig. 9 Contour plots of the ion flow velocity for the whole PSI-1 device (left), the anode region (middle) and the region just above the neutralizer plate (right). The arrows show the direction and the absolute magnitude of the ion flow velocity near the anode.

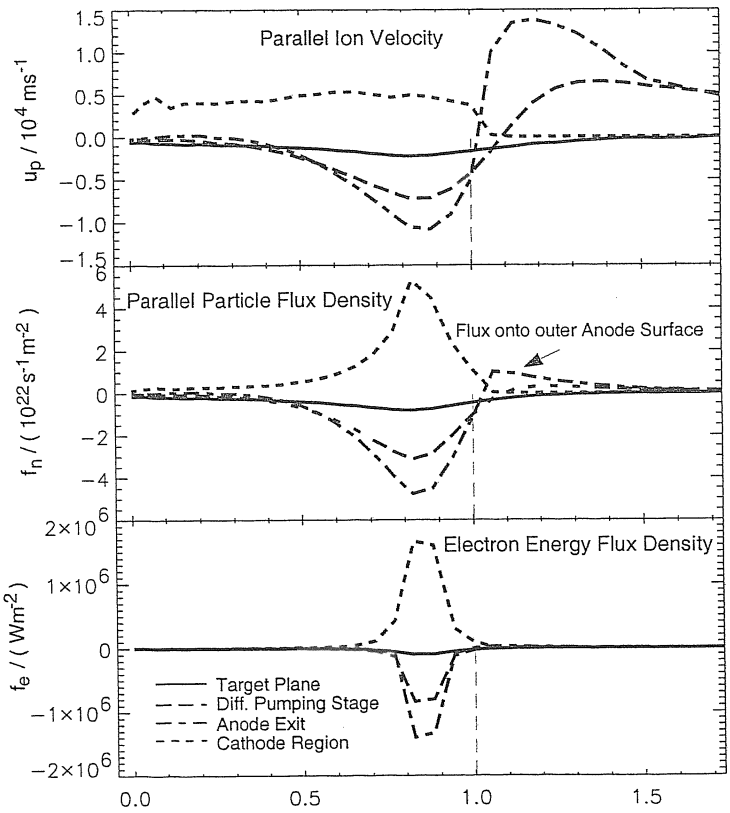

Fig. 10 Radial profiles of the particle velocity and flux density and the electron energy flux density at different axial positions projected along the magnetic flux lines onto the normalized radial coordinate at the target plane. Positive values of u_p, f_n and f_e mark the flow direction to the cathode.

The contourplots in Fig. 9 give an overview of the ion streaming velocity for the whole PSI-1 device and for the anode and dump regions, respectively. The ion velocity varies strongly axially and radially within the device. The stagnation line (zero velocity) extends from the middle of the energy source region at the periphery up to out of the anode exit in the centre of the plasma. In direction of the cathode the velocity increases continuously and reaches a maximum of about $10^4 m/s$ ($mach \approx 1.5$) at the cathode bottom. On the other side of the stagnation line, the ion velocity (actually the parallel velocity) is strongly modulated by the inhomogeneity of the magnetic field. It is minimum in the target plane where it varies between $600m/s$ (in the plasma center) and $2200m/s$. A maximum of $u_p \approx 3.5 \times 10^4 m/s$ ($mach \approx 2.5$) is reached at the neutralizer plate.

The existence of a hollow radial $n_e(= n_i)$ profile over a long part of the plasma column has a pecular consequence for the flow pattern of deuterium plasma which is not found for heavy noble gases where the profiles become already monotoneous near the anode exit. Due to inward radial diffusion the density (and the pressure) in the center of the plasma column downstream of the anode becomes larger than in the anode region itself causing an ion backstreaming near the plasma axis into the anode. This effect is only weak in the case of Figs. 9,10, but becomes more pronounced for lower overall densities. Outward diffusion, on the other hand, always occurs and gives also rise to an appreciable ion flux backward to the outer edge of the anode (see Figs. 9,10).

In contrast to the particle flux which is spread over the whole plasma cross section the parallel electron energy flux is limited to a very small radial plasma layer as shown by the extremely peaked profiles in Fig. 10. This is a consequence of the hollow T_e profile in conjunction with the nonlinear dependence of the classical heat conductivity on T_e ($\kappa_{\|} \propto T_e^{5/2}$) which decreases strongly with the radially falling temperature.

Some striking aspects of the code results such as the non-monotoneous axial plasma flow or the occurrence of a localized strong axial gradient of the electron temperature (Fig. 11) can be explained by the hydrodynamic properties of the plasma in the inhomogeneous magnetic field.

Fig. 11 shows axial profiles of some basic plasma parameters along a coordinate line which intersects the external electron energy source near the inner anode boundary. The radius R of the corresponding flux surface as a function of the magnetic field strength is also given in this figure.

The dominant driving force for the axial plasma motion is the pressure gradient. The pressure maximum (defining the flow stagnation point) is near the external energy source where the ionization rate due to the fixed source temperature ($T_{e,source} = 12eV$) is high. Because of enhanced local recycling in front of the cathode bottom, however, the density and pressure maximum is shifted axially relative to the source in the direction of the cathode. The basic ion sinks and the pressure minima are at the cathode bottom and the neutralizer plate, where the plasma is neutralized.

As may be seen from Fig. 11 , the plasma flow between the anode and the neutralizer plate is clearly modulated according to the variing cross section of the plasma column. Because of particle flux conservation the ion velocity must increase where the cross section becomes small (at the position of the anode, the diaphragm and the dump) which requires a steepening of the pressure gradient and vice versa. The ion temperature, on the other hand, is closely connected to the variing ion velocity by the reciprocal exchange of convective (E_{kin}) and thermal (T_i) energy. The sum E_{kin} + T_i is obviously nearly constant along the column. Ion energy sources via ion-neutral processes or the energy equipartition term $k(T_e - T_i)$, $k \propto Z_i^2 m_i^{-1} n_i n_e / T_e^{3/2}$, are small outside the anode and have no noticeable effect on T_i (and T_e).

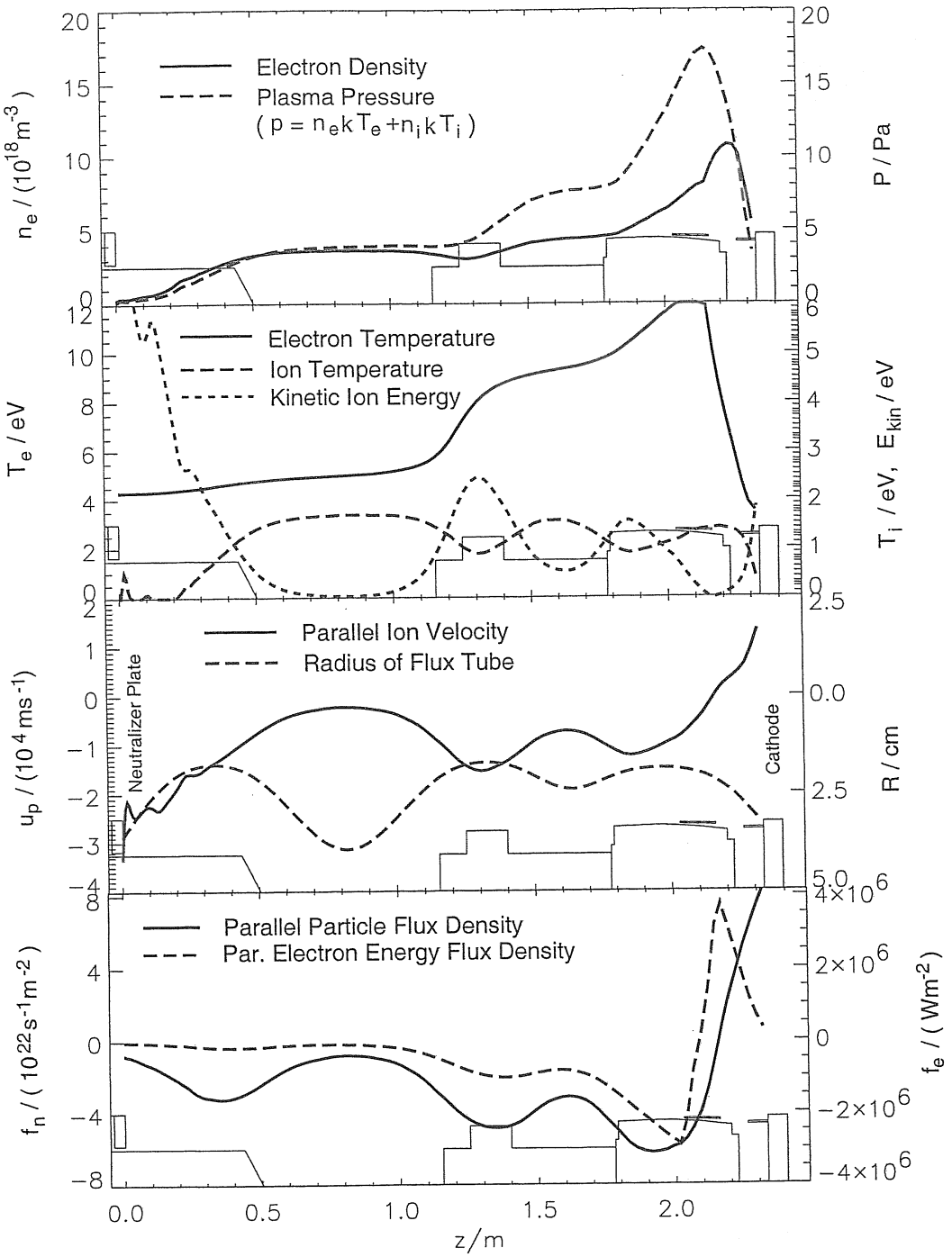

Fig. 11 Axial plasma profiles along a coordinate line (magnetic flux surface) which passes through the external electron energy source (see text). A scheme of the device (cf. Figs.1,2) is included in each figure for better orientation.

This energy coupling between electrons and ions is most effective in the anode region where the density and temperature difference are high (Fig. 12). The dominant energy loss term for electrons outside the anode is due to the interaction with the neutrals which is about two orders of magnitude higher (Fig. 12).

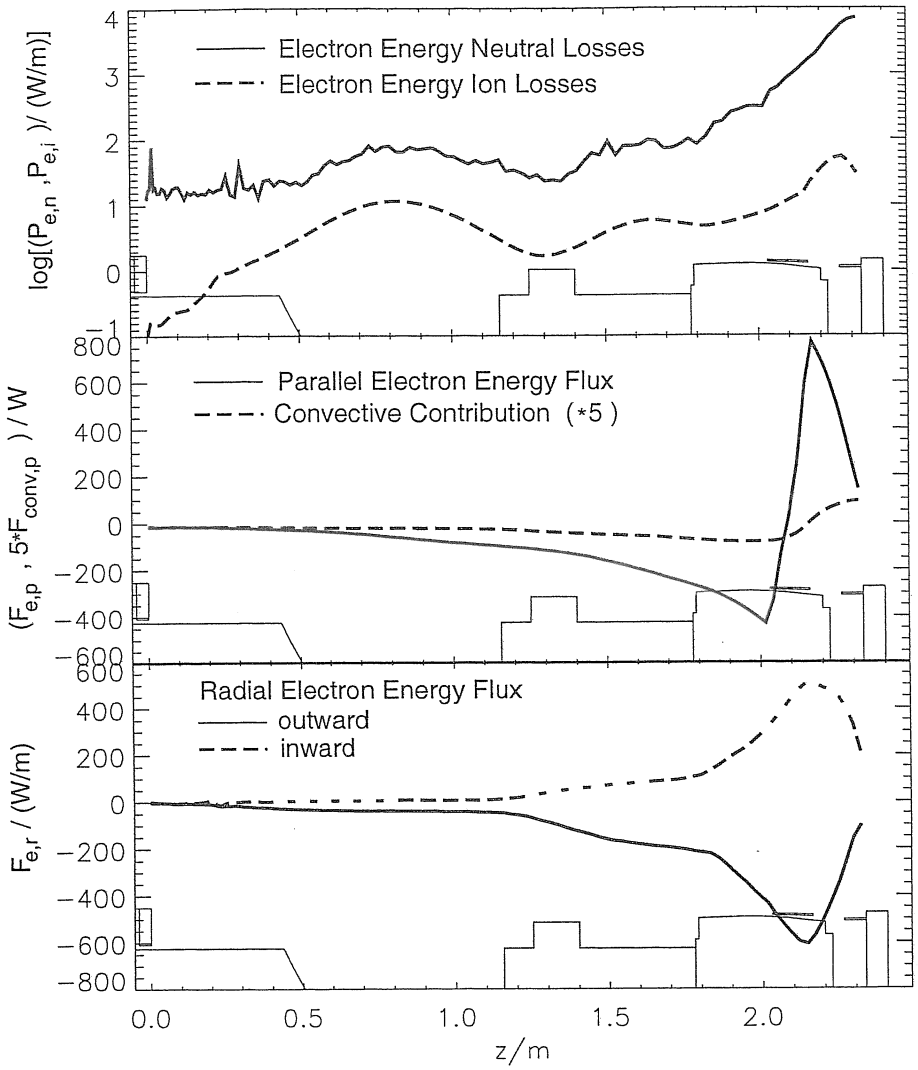

Fig. 12 Parallel electron energy fluxes and electron energy losses per meter due to the radial heat flux and the electron interaction with neutrals and ions, respectively, for a magnetic flux tube passing through the external electron energy source (see text).

In order to see what induces the steep electron temperature decrease near the diaphragm we consider the total energy fluxes and losses within a magnetic flux tube passing through the external energy source (Fig. 12). Here, the flux tube is defined by the cylindrical shell radially bound by two consecutive coordinate lines.

First we notice that, in contrast to the energy flux density in Fig 11, the total parallel electron energy flux decreases monotonously outside the source region mainly due to energy losses to the neutrals (ionization, dissociation) and radial heat conduction. The flux is essentially determined by parallel heat conduction, the convective contribution varies only between 15% of the total flux in the dump region and less than 5% near the cathode. The parallel ion energy flux is much smaller.

The electron energy losses to the neutrals and to the ions are volume processes described by loss densities ($p_{e,n}$, $p_{e,i}$). The losses per meter flux tube length ($P_{e,n} = p_{e,n} s_x$, $P_{e,i} = p_{e,i} s_x$) vary with the cross section s_x of the flux tube ($s_x \propto R \times \Delta_B$) which explains the relative maxima where the magnetic field strength becomes weak and the radial separation Δ_B of neighbouring

magnetic flux surfaces is large (Fig. 12).
The radial energy losses per meter ($F_{e,r}$), on the other hand, are only proportional to the surface of the flux tube, i.e., proportional to the radius R of the plasma column. (However, they depend also on the radial gradients and, hence, are locally enhanced at those axial positions where the plasma column narrows.) Although the variation of the radial losses is small and practically not reflected in the uniformly decreasing curve for the parallel electron energy flux in Fig. 12 they may induce the pronounced steep gradients of T_e near the diaphragm and the anode, respectively.

To see the different effects of these losses on T_e, we relate each energy loss terms to the electron energy content per meter of the flux tube, $n_e T_e s_x$, which is also proportional to s_x. While $P_{e,n}/n_e T_e s_x = p_{e,n}/n_e T_e$ shows no modulation with the column radius (Fig. 13), one finds maxima for the radial losses $F_{e,r}/n_e T_e s_x$ at those axial positions where Δ_B and hence, the radius of the plasma column is minimum. This will cause a locally enhanced decrease of T_e. Because of the nonlinear dependence of the parallel heat conductivity on the electron temperature, ($\kappa_\parallel \propto T_e^{5/2}$) this (possibly small) local drop of T_e may require an even steeper axial gradient for T_e at these positions in order to maintain the practically continuous parallel electron heat flux. (This effect becomes still more pronounced for lower plasma densities.)

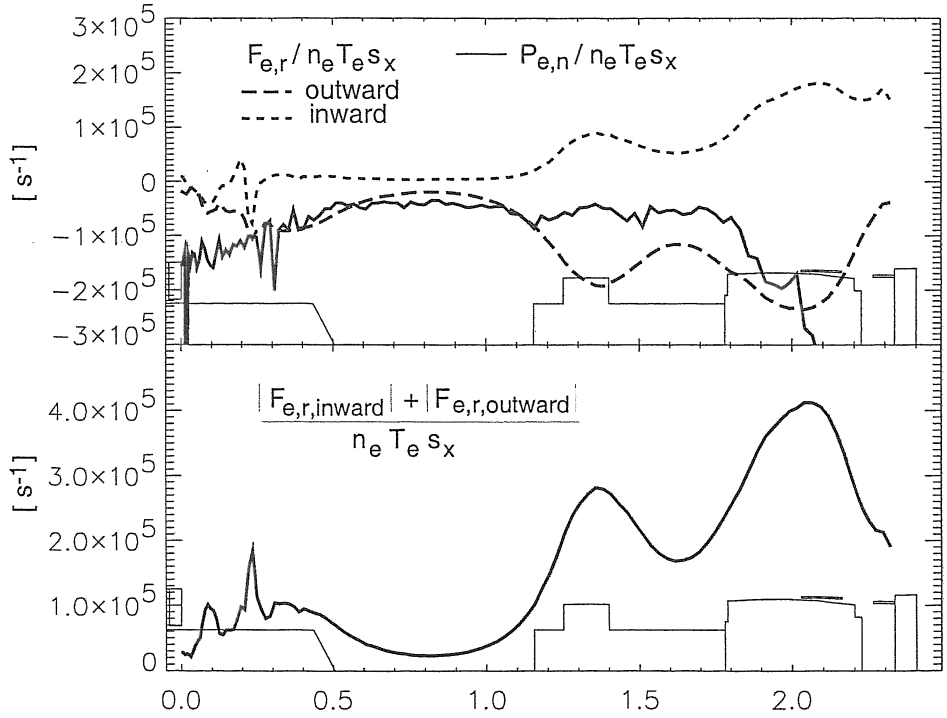

Fig. 13 Ratio of the radial energy radial energy losses (electrons: $F_{e,r}$, neutrals: $P_{e,n}$) and the internal electron energy per meter along a magnetic flux tube (electron energy exchange frequency). The ratio shows the relative importance of these losses for T_e in dependence on the magnetic field strength. It is also essential for the steep axial decrease of T_e near the diaphragm (Fig. 11)

3.3 Neutrals

In the model, the neutrals are appropriately described by the Eirene Monte-Carlo code according to the following scenario: The only external source of neutrals are D_2 molecules

of approximately room temperature which enter the PSI device through a concentric hole in the cathode bottom. The external sinks of neutrals are given by the pumps in the differential pumping stage and at the target chamber. External source and loss rates are equal in steady state. Within the device, the neutrals interact with the plasma (electrons) via dissociation, ionization and elastic collision processes. At the surfaces the ions are neutralized and reemitted as atoms or molecules. Atoms hitting the wall are either reflected (according to the TRIM or MARLOW database) or recombine and leave the surface as thermal molecules.

The following results refer to the same model parameters as considered in the previous section. Figs. 14 and 15 show contourplots and axial profiles of the mean free path length of atoms, the ionization rate (production of D^+) and the electron energy loss rate due to the interaction with the neutrals (dissociation, ionization, excitation/radiation and elastic collisions). The mean free path of the atoms with respect to ionization is defined here by $l_a = \sqrt{2kT_a/m_a}\; n_a/s_{ion}$, where s_{ion} is the ionization rate per volume and the index 'a' refers to atoms. It varies between $10\,cm$ in the hot and dense anode region and more than $10\,m$ near the target plate. Apart from the cathode region, the mean free path lengths of the atoms exceed the radial dimension of the device under the actual discharge conditions. Local recycling occurs only between the external energy source and the cathode plate leading to an increase of the plasma density in that region (cp. Fig. 11). In the other part of the device many successive wall reflections of atoms take place and the recycling effect is distributed over the whole radius and over a long axial distance.

The electron-neutral processes depend sensitively on the electron temperature and, therefore, are concentrated radially to the thin hot plasma layer which is magnetically connected to the external energy source in the anode and axially to the primary energy source region inside the anode. The volume integrated ionization rate outside the anode is about 11% of the total rate, for the total electron energy loss this ratio is about 16%. In the mean, a hydrogen molecule is several times dissociated by electron impact and recombined at the surfaces before it is ionized to yield a H^+ ions. Thus, roughly one third of the electron energy loss is directly tranported by the atoms to the walls of the device (see also ch. 3.4).

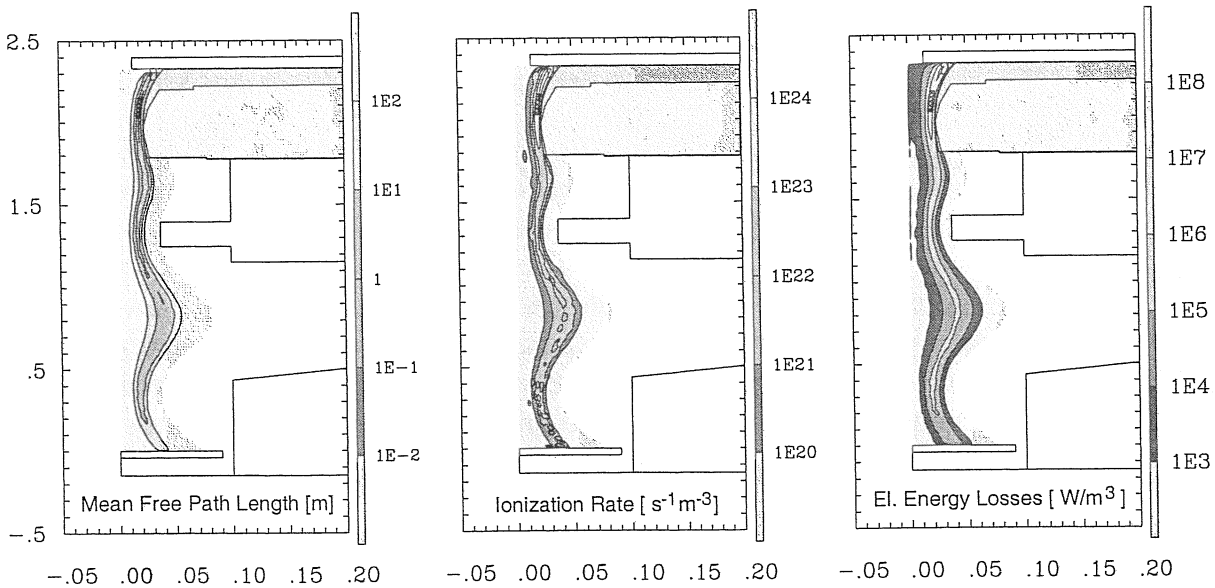

Fig. 14 Mean free path length of atoms, ionization rate and electron energy loss rate due to interactions with neutrals

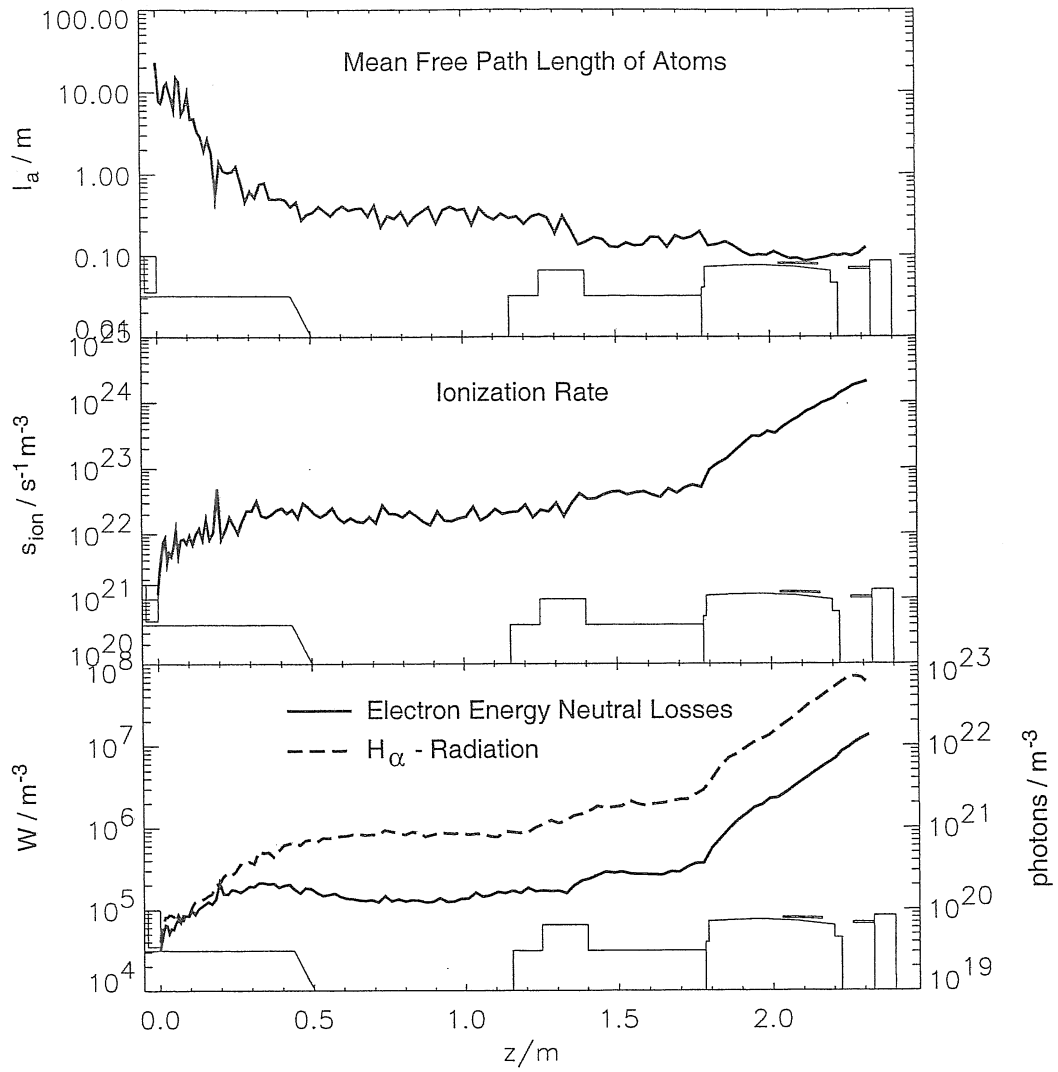

Fig. 15 Plasma neutral interaction. Axial profiles along a field line passing through the external electron energy source at the anode (radial position of maximum electron temperature).

The contourplots in Figs.16 give an overview of the molecular and atomic density and the ionization ratio in the whole PSI-1 device; some radial profiles including experimental results are shown in Figs. 17 and 18. The experimental data were obtained for discharges which are comparable with the modelled plasma state.

The calculation shows that in the case of deuterium the plasma is only partially ionized everywhere in the device. In the target plane, the degree of ionization is about 50% which agrees with experimental findings / 12 /. Roughly half of the neutral deuterium is dissociated. The radial profiles of the neutrals are determined by their corresponding sinks and sources at the walls of the device and within the plasma volume, respectively. The D_2 density (which is maximum near the gas inlet hole) has a radial maximum at the outer side of the plasma column where D_2 molecules are thermally emitted from the walls due to atom recombination. Inside the plasma the D_2 density decreases due to dissociation of the molecules. This general radial behaviour is in agreement with the experimental D_2 profile (Fig. 17) spectroscopically derived

in / 12 / from the Fulcher$_\alpha$ emission / 13 /. (The outmost point of the experimental curve indicating a density decrease is related to experimental inconsistencies / 12 /.)

The radial density profiles of the D atoms (born within the plasma by charge exchange and dissociation of D_2 molecules), on the other hand, should behave oppositely. Actually they are rather flat because of the long mean free path length of the atoms which is a consequence of the higher average energy of about 1–2eV (see Fig. 18). The radial region where the volume production rate of atoms is maximum (according to the radial maximum of the electron temperature and density) is only weakly reflected in the radial profiles. This is in certain contradiction to the experimentally measured atomic density profile shown by the asterisks in Fig. 17, which increases significantly at the center of the plasma / 12 /. In the experiments, the atomic density was found to consist of two components characterized by different temperatures: a relative low "background atomic density" of about 0.6eV and charge exchange atoms having ion temperature (7.3eV) which are responsible for the central density increase. The calculated atomic temperature of about 1–2eV in Fig. 18, on the other hand, is the average energy of atoms which originate from Franck-Condon dissociation, charge exchange processes, ion recombination and multiple surface reflection. Such an high ion temperature is not obtained by the model where the ions gain their energy mainly by equilibration with electrons.

The experimental results were derived from passive spectroscopy of the H_α emission (H_β measurements yield corresponding results), which however, also requires the knowledge of the electron temperature and density profiles. The latter have been simultaneously measured by a fast Langmuir probe. Possible reasons for the difference in the atomic density curves may primarily be due to differences between the calculated and measured electron density and temperature profiles in Fig. 8 (in particular the dependence on the electron temperature is very crucial for the interpretation of the measurements in the actual low temperature range at the plasma center) but also due to differences in the set of atomic processes included in the numerical model and for the experimental determination, respectively. Further investigations are necessary.

In contrast to the atomic density profile, the H_α radiation (Fig. 18) is radially strongly peaked because of the sensitive dependence of the rate coefficient for electron impact excitation on the electron temperature in the actual range of T_e (Fig. 8). In the axial direction the emission rate decreases over about two orders of magnitude from the anode region to the target plane (Fig. 15).

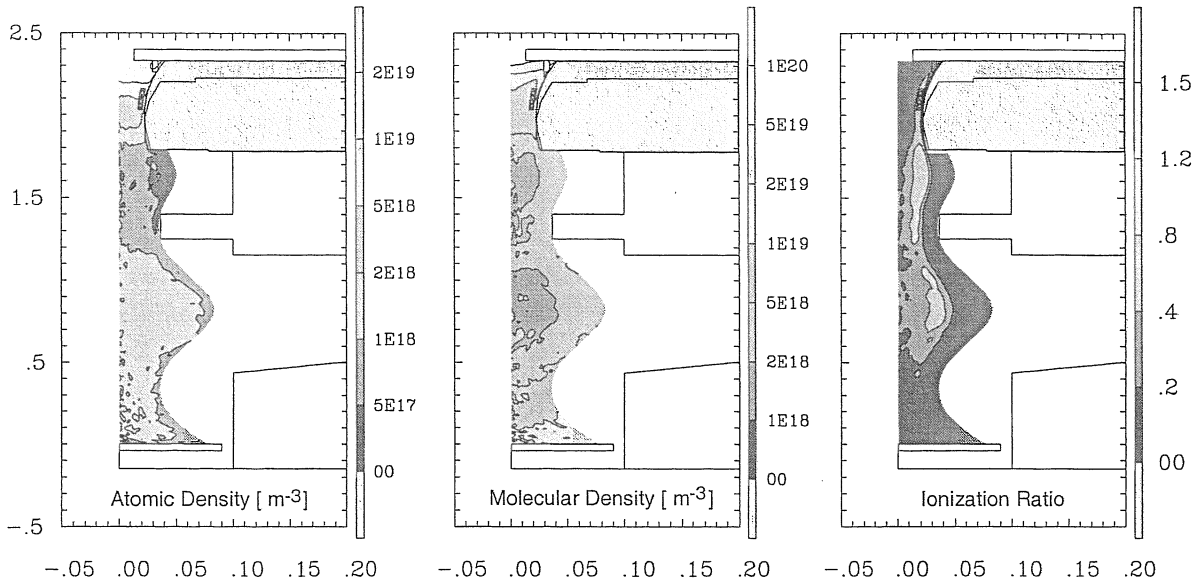

Fig. 16 Contourplots of the neutrals density and the ionization ratio

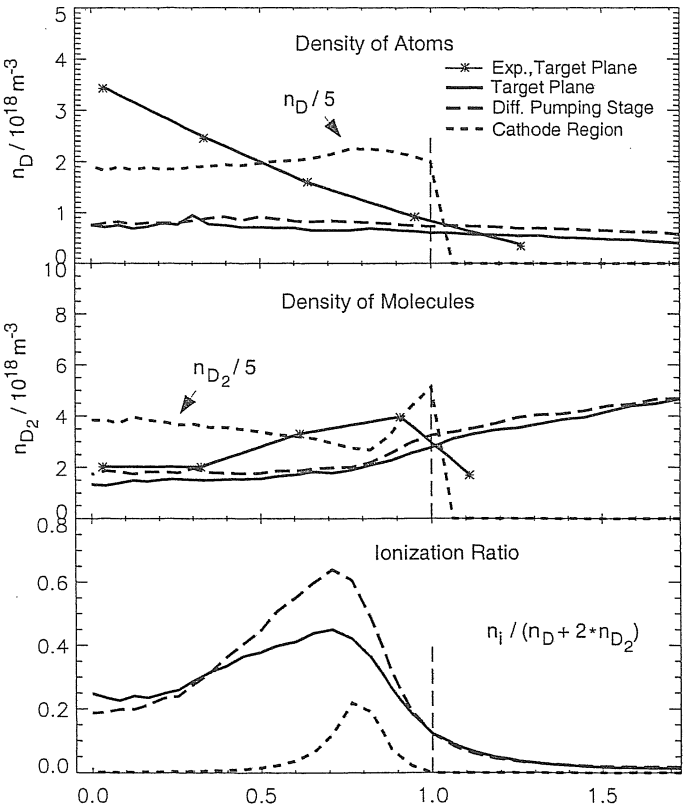

Fig. 17 Radial profiles of the neutral density and the ionization ratio at different axial positions. The experimental curves are taken from / 12 /. The ionization ratio is defined in the lower figure.

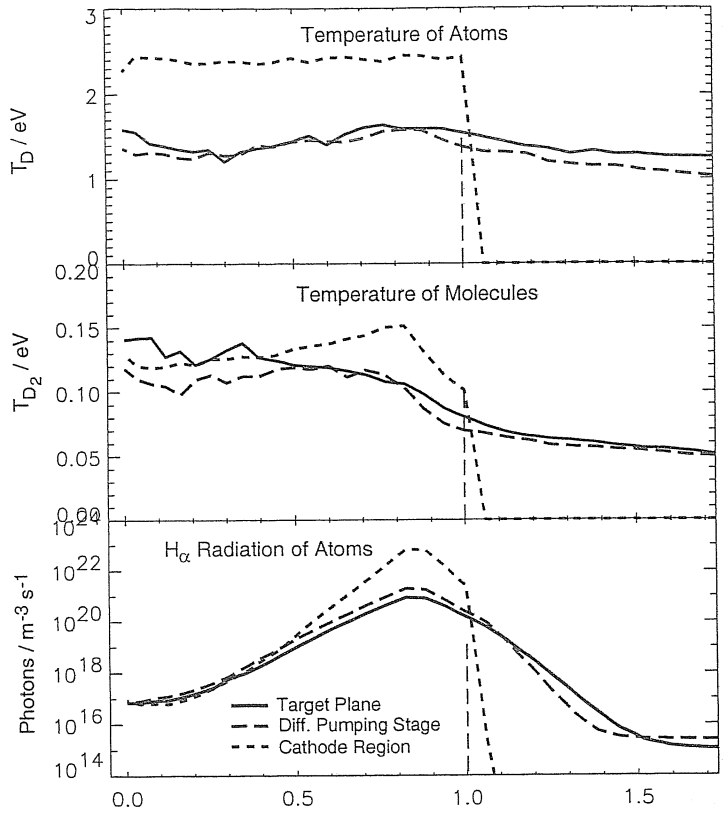

Fig. 18 Radial temperature profiles of atoms and molecules and atomic H_α emissivity at different axial positions

3.4 Energy Flow in the PSI-1 Device

The code offers the possibility to trace the flow of the input electron energy via the different physical processes to the neutral and charged plasma species and to calculate the local power load for the surfaces of the device. This load distribution has been experimentally investigated in / 14 / for hydrogen and some noble gas discharges in a wide range of total input power (5kW to 25kW) using calorimetric methods. In the case of hydrogen it was found, that about 86% of the total electric input power remains within the anode-cathode region, the most loaded part being the anode where about 75% of the total power is absorbed; the rest leaves the anode exit. The relative energy distribution onto the different modules of the device was found to be practically independent of the total discharge power. These observations will be compared with our code results.

In our model, the energy load of each surface is given by the sum of the following three components: (i) The energy deposited by recycling neutrals, (ii) in the case of surfaces touching the plasma, the conductive and convective energy fluxes of electrons and ions including the ion recombination energy minus the energy carried away by the recombined neutrals, and (iii) the radiation load. The first two components are shown in Fig. 19. Since the radiation source is strongly localized near to the anode surface (cp. the profiles for the H_α radiation in Figs. 15 and 18) , the total radiation that is emitted in that region (642W), should be added to the anode load. The energy radiated in the whole device outside the anode is only about 53W ($\approx$ 7%).

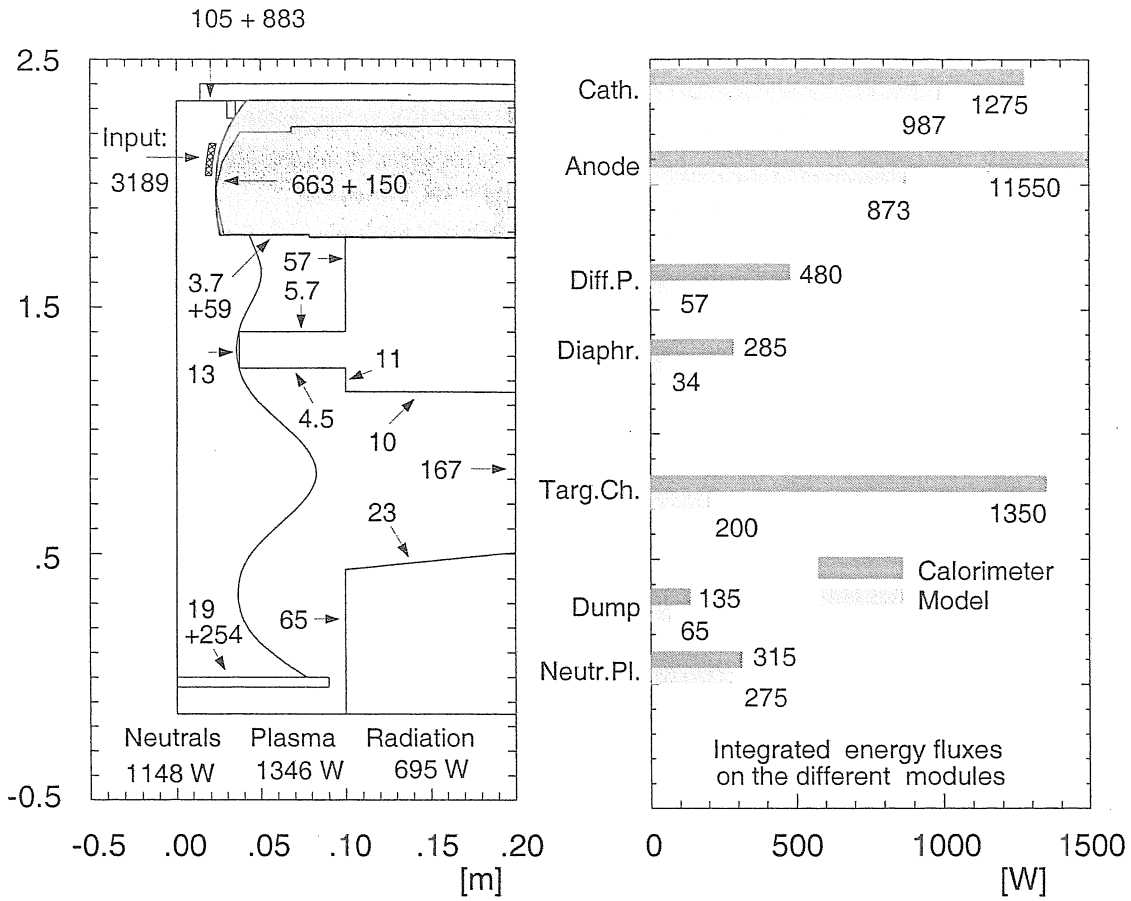

Fig. 19

Left: Distribution of the total input electron energy on the different surfaces of the PSI-1 device as obtained from the B2–Eirene calculation. The first number gives the energy (in [W]) deposited by the impinging flux of atoms and molecules. The added number is the absorbed part of the energy fluxes of electrons, ions and the recombination energy. The total energy transported by the neutrals, the plasma and by radiation is given in the bottom of the figure.

Right: Steady state energy fluxes onto the cathode, the anode, the differential pumping stage, the diaphragm, the target chamber, the dump and the neutralizer plate obtained from the model (without radiation load) and measured experimentally by calorimetric methods / 14 /, respectively (see text).

In the right hand part of Fig.19 we compare our results with the available data for a 15 kW hydrogen discharge at a gas influx rate of 3.7×10^{19} molecules/sec / 14 /. Most of the experimental total input power is directly transfered by the electric current to the anode. This effect is not included in our model. A direct comparison, however, should be reasonable for the other surfaces in Fig. 19 which are charged via the (ambipolar) plasma and heat flow of the neutrals. For the target plate, which is farest from the hot anode and directly heated by the parallel energy flow, we find nearly the same load in the experiment as in the model. In the experiment, this plate (as well as the anode and cathode) reaches a calorimetric steady state after few minutes. For the other sections of the device closer to the anode the ratio between

the experimental and the calculated energy load increases continuously, from a factor of two at the dump up to a factor of about 10 at the differential pumping stage. Common to these parts is that the energy transport from the plasma to the surfaces is accomplished via neutrals (the radial ion flow is very small at the surfaces radii) and that the experimental thermal steady state is reached only after 40–50 minutes. The difference between the calculated and measured total energy flux outside the anode, respectively, is 1881W; i.e., only about 1/3 of the calorimetric measured flux of 2565W is obtained by the numerical calculation. Hence, the energy transport by the neutrals may be strongly underestimated by the model, which would coincide with the too low density of energetic charge exchange neutrals obtained by the calculations as compared with the experiment, or there must be still another mechanism, not included in the model, which transports the energy to these surfaces. This massive discrepancy could also explained by strong impurity radiation, which, however, is not observed in the experiments. Other shortcomings of the transport processes considered in the present model or heat conduction along the material of the vessel are unlikely to account for it. Characteristic impurities observed in PSI–1 are above of all copper, which is sputterd from the anode, but also carbon, oxygen and nitrogen. Bolometer measurements – not done at PSI-1 up to now – would clarify this problem. Further calculations with the B2–Eirene model will include the main impurity species.
Finally it should be noted that according to the model calculation practically the whole energy flux leaving the throat of the anode is carried by the plasma, the energy outflux due to the neutrals is very small (about 2W in the considered case).

4. Summary

The B2–Eirene code package was used to model numerically a deuterium plasma including the neutrals in the PSI-1 device. Simulating the actual arc discharge in the anode-cathode region by an empirical plasma energy source, where the source temperature and dimension are parameters which have to be fitted, the (field-free) code could be applied to the whole device thus avoiding to prescribe boundary conditions at the anode exit. This source is localized to a small radial layer near the inner anode surface (according to the localization of the discharge current for the particular design of the anode and cathode) and gives rise to pronounced hollow density and temperature profiles.

The radial plasma profiles observed along the plasma column are determined by the concurrent action of radial diffusion, axial plasma flow and the ionization of the neutral gas background. Moreover, they are clearly modulated by the inhomogeneity of the axial magnetic field. This can mainly be explained by hydrodynamic effects due to the varying flux tube cross section. In this way, by the particle flux conservation, the ion flow velocity and plasma density are directly coupled with each other and to the cross section, but also the electron temperature is strongly influenced because of the proportionality of the radial energy losses to the column radius and the sensitive (nonlinear) dependence of the parallel electron heat conductivity on T_e.

Several classical and empirical radial transport models have been tested by comparing measured and calculated plasma profiles. Other than in fusion devices, the (self-consistently) calculated classical diffusion coefficients ($D_i \propto n_0 B^{-2}$) reach values of the order of $1 m^2/s$ (since the magnetic field is very low and the neutral density fairly high in PSI-1) and may be considered to describe the diffusion behaviour. Thus, for example, the classical ambipolar diffusion may essentially explain the radial profile near the density maximum, but in the outer plasma region much higher diffusion coefficients would be required (in the anode shadow even stronger increasing than $1/n_i$) in order to verify the experimental profiles. A reliable statement, however, whether one of these different diffusion models is valid and in which plasma region, is not possible at this time. Most calculations in this paper, aimed at a quantitative test of the code, have been done, therefore, assuming $D_i = const. = 0.5\, m^2/s$ within the main plasma column and $D_i \propto 1/n_i$ outside.

To test the code quantitatively, an actual discharge has been modelled and the results were compared with the experimentally observed profiles for the charged as well as the neutral species. A good agreement was found between the calculated and the measured electron density and temperature in the target chamber for the predominant radial plasma region. The measured (hollow) profiles, however, are more flat than the calculated ones. In case of the density, this may indicate that the radial diffusion coefficient is not properly chosen, in particular far outside in the anode shadow. In the central plasma the measured density is by a factor of $\lesssim 1.5$ higher than the calculated value. The differences between the calculated and measured electron temperature profiles in these regions are more serious; in the larger part of the central plasma the density measured by a fast Langmuir probe exceeds the calculated one by a factor of $2 \div 3$. The mechanism leading to this strong inward energy transport is not clear yet and will be subject to further model developments. Some principal shortcomings of the code, however, the neglect of the radial electric field and the plasma rotation, can also falsify the energy balance. In particular the ions generated in the plasma column can gain an appreciable amount of energy in a radial electric field. The actual importance of these defects need still to be clarified.

Not yet clear are also some deviations found for the neutral species. The calculated and measured D_2 densities differ by a factor of $1.2 \div 2$ but both profiles show the expected decrease toward the plasma center. The D density profiles deviate from each other in particular near the column axis, where the measured atomic density is by a factor of 3 higher. While the code predicts rather flat profiles due to the long mean free path of atoms which have a calculated (mean) temperature of about $1.5\,eV$, the measurements by passive spectroscopy revealed that the locally enhanced atomic density at the plasma center is due to charge exchange atoms having a temperature of $7.3\,eV$. This discrepancy can be (at least partly) a consequence of the low ion temperature obtained by the model. The absence of these atoms may also be responsible for the too small calculated energy flux to the vessel of PSI-1.

Summarizing the results one may state that the presented model is able to describe quantitatively the plasma in PSI-1 in the predominant radial plasma region, i,e., in the radial vicinity of those flux surfaces where the plasma is generated. The deviations between code predictions and the experiment concern the radial profile outside this region and are within reasonable limits. Further improvements should be achieved by a more realistic radial transport model and the clarification and proper inclusion of the ion kinetics.

Acknowledgment

The authors thank Prof. Dr. G. Fußmann for supporting this work and for drawing attention to the importance of internal fields for the radial transport due to the specific discharge conditions in the PSI-1 device.

References

/ 1 / Behrendt, H., Bohmeyer, W., Dietrich, L., et al., Proc. 21st EPS Conf. on Contr. Fusion and Plasma Physics (Montpellier, 1994), p III-1328
/ 2 / Schmitz, L., Lehmer, R., Chevalier,G., et al., J. Nucl. Mat. (1990) 522
/ 3 / Ezumi, N., Aoki, K., Nishijima, D., et al., "Investigation of hydrogen plasma detachment in the divertor simulator NAGDIS-II", 25th EPS Conf. on Contr. Fusion and Plasma Physics (Prague, 1998), Abstracts p II–724
/ 4 / Reiter, D., J. Nucl. Mat. 196–198 (1992) 80
/ 5 / Schneider, R. et al., J. Nucl. Mat. 196–198 (1992) 810
/ 6 / Braams, B. J. "Computational Studies in Tokamak Equilibrium and Transport, PhD thesis, Rijksuniversiteit, Utecht, Nederland, 1986
/ 7 / Braams, B. J. Technical Report 68, Next European Torus, 1987
/ 8 / Reiter, D. et. al. J. Nucl. Mater. 220–222 (1995) 987, PSI 94 Mito
/ 9 / Kastelewicz, H., Reiter, D., Schneider, R., et al., 24th EPS Conf. on Contr. Fusion and Plasma Physics (Berchtesgaden, 1997), p IV-1805
/ 10 / Kastelewicz, H., Reiter, D., Schneider, R., et al., 23rd EPS Conf. on Contr. Fusion and Plasma Physics (Kiev, 1996) p II-803
/ 11 / Bachmann, P., Reiter, D., "Kinetic Description of Elastic Processes in Hydrogen-Helium Plasmas", Contrib. Plasma Phys. 35 (1995) 45–100
/ 12 / Meyer, H., "Analysis of the Plasma Rotation in a Magnetic Configuration", Thesis, Humboldt-Universität zu Berlin, printed as IPP Report no 8/14 (IPP8/14), 1998
/ 13 / De Graaf, M., "A New Hydrogen Particle Source", Thesis, Technische Universität

Eindhoven, 1994
/ 14 / Fuchs, T., "Bestimmung des Energiehaushaltes und des Leistungseintrages in Targets am Plasmagenerator PSI-1", Diploma thesis, Humboldt-Universität zu Berlin, Juni 1996